International Research Journal of Earth Sciences _____ ISSN 2321 – 2527
Vol. **6(12),** 1-11, December **(2018)** *Int. Res. J. Earth Sci.*

Soil-radon fluctuation and local climate parameters - a multifractal cross-correlation study

Alpa Kar, Shankha Sanyal* and Dipak Ghosh
School of Studies in Environmental Radiation and Archaeological Sciences, Department of Physics, Jadavpur University, West Bengal, India
ssanyal.sanyal2@yahoo.com

Available online at: www.isca.in
Received 5th September 2018, revised 20th November 2018, accepted 15th December 2018

Abstract

The use of Radon (Rn) gas as an effective precursor for earthquake detection have been well established, but the correlation of Rn time series with other climatic parameters such as rainfall, humidity is often neglected. But these parameters do play an outstanding role in the domain of pre-seismic surveillance. Fractal analysis of complex time series data provides efficient means of characterizing and quantifying the long range temporal correlations present in the signal. In this work, we have applied robust nonlinear tools like Detrended Fluctuation Analysis (DFA), Multifractal DFA (MFDFA) to characterize time series data of Rn, temperature, rainfall and humidity for the last 10 years ranging from September 2005-August 2014. Also, we have used the Multifractal Detrended Cross-Correlation Analysis, MFDXA for the assessment of the degree of association present between the different time series data mentioned above. The results show that the Rn time series has the strongest amount of correlation with the temperature time series data. This study with rigorous methods presents interesting results that should be taken care of as a caution before confident identification of occurrence of earthquakes.

Keywords: Rn monitoring, temperature, rainfall, Hurst exponent, MFDFA, MFDXA.

Introduction

Radon is a chemical element bearing a symbol Rn and having atomic no. 86. It is a radioactive noble gas occurred naturally in the environment and is obtained from the decay of Ur via Ra. Rn has 39 isotopes from ^{193}Rn to ^{231}Rn but among them the most stable one is ^{222}Rn having a half-life of 3.82 days. Rn has only 3 radioactive isotopes, namely: ^{222}Rn (3:82d), ^{220}Rn(55s) and ^{219}Rn(~ 4s), in natural environment. In nature, the 4 isotopes ^{218,219,220,222}Rn arise as a degrading product of ^{218}At, ^{223}Ra, ^{224}Ra, and ^{226}Ra respectively[1].

Rn is the main cause of most of the radioactivity in the atmosphere at sea level. As a radio-active and chemically inactive gas, Rn releases from soil and rupture of the rocks under the substratum in the ground. In soil, 10% of the Rn is diluted to the atmosphere[2]. Besides soil, Rn also exists in lumped rock, building materials, subterranean and shallow waters[2,3]. Due to a number of factors like distribution of Ur (especially ^{226}Ra in the same series) in the soil and in substratum, soil porosity, humidity, micro-cracks of substratum, rainfall, air temperature etc the migration of Rn upwards are affected. While all generated Rn atoms are diluted in fluids, only a percentage of Rn emerge porous media and fragmented rock and dissolve into the pore's fluid[1,3].

Different methodologies have been proposed in the literature for monitoring non-tectonic variables of both geophysical and geochemical nature, of which, Rn gas monitoring proved to be very promising among all other methods, due to its connection with the highly deformed tectonic region and various advantages in its detection as well. For the prognosis of earthquakes, Rn has also been utilized extensively. Rn drifts from its production region and is almost chemically inactive. It can be easily detected even at low levels[1-3].

The earthquake is a trembling of the ground usually stimulated by the liberation of underground tension along the rifts. ^{222}Rn gas is constantly formed within the rock of the earth as an intermediary decay outcome of the ^{238}U radioactive sequence. The gas fluxes along the faults or fractures during the stress-strain occurring in the earth's crust as a result of an earthquake. These transport the Rn gas from its birthplace towards the surface of the earth[5]. The half-life of Rn gas [$T_{1/2}$ = 3.82 days] is on the higher side and hence it can spread at the decreasing rate in ground soil. Hence the Rn concentrations that are counted must be several kilometres away from the original source. The observation of Rnin consistency analogous to the seismic activity has been the food for study in a number of experiments around the globe[6,7]. Different instruments were used for this purpose like alpha guard, ZnS(Ag) detector, Lucas type scintillation chamber, SSNTD[8-13]. Active fault areas like Antarctica, Mexico, East Europeetc. have proven to be an important indicator in the use of radon flux in pre-seismic event detection[14-16].

Because of increase in crustal confining, Rn anomalous concentration may be induced, that extract the Rn gas into the atmosphere at an intensify rate before an earthquake, according to King's (1978) compression mechanism[17]. Hauksson reported

that for earthquakes of higher magnitude, Rn anomalies occur at larger epicentral distances, while the precursor time is lesswhen the distance between the epicenter and the Rn monitoring station is small[18]. For seismic events, Rn anomaly can act as a precursor. Hence the time series of Rn fluctuation pattern bears a lot of significance. Walia have found a stronger relationship between Rn incongruity and seismic parameters in N–W Himalaya, a distinct increase in ^{222}Rn concentration in the thermal spring of Bakreswar have been observed before the tsunami in Indonesia in 2004 having 9.1 magnitude earthquake[19-21]. Earthquake predecessor study associating soil and subsoil water Rn measurement has been reported by Ramola[22]. Pre - seismic trademarks in the coast of Rn gas, in the lower part of the Himalayan region at an elevation of 800 meters have been observed by Barman *et.al* overhead the mean sea level[23]. To study the reservoir-triggered earthquakes in the Koyna–Warna region, alongside the west coast of India, Reddyhave performed a study on soil radon[24]. Before the current earthquakes in Nepal and in the eastern part of India mainly on 25thof April in Nepal having magnitude 7.8[25], exceptional variations in the datasets of radon have been noticed during the track period.

Thus, we have seen that a number of earlier works which supports the fact that Rn anomaly provides important clues as a precursor of earthquake. Radon fluctuation has been identified by celebrated nuclear scientist Charpak as the most efficient precursor of earthquake. However this fluctuation is often vitiated by local climatic parameters such as temperature, rainfall, relative humidity etc. But these parameters are not often taken into consideration from the point of view of any rigorous scientific analysis. For the first time, we have tried to correlate the changes of local climatic parameters with radon gas anomaly using latest nonlinear techniques. We present in this paper a correlation study in non-linear scenario between radon concentration and climate parameters like temperature, rainfall, humidity etc. using current predicament of the art skills such as MFDXA (Multifractal Detrended Cross-Correlation Analysis)[26].

The word 'fractal' was first introduced by Beniot Mandelbrot[27] from the Latin adjective fractus (the corresponding Latin verb frangere means "to break" to create irregular fragments) for indicating objects whose complex geometry cannot be distinguished by an integral dimension. Its ability to describe the irregular or shattered shape of natural features as well as complex objects that cannot be represented by traditional Euclidean geometry is the main attraction of fractal geometry.

The Detrended Fluctuation Analysis technique extracts the scaling exponent corresponding to long-term correlated sequemce[28-31]. The other remarkable techniques[28-32] are the time-evolvement of the fractal acreage, the Hurst exponent and the materialistic difference of heterogenous metrics of degeneration respectively. It is to be noted that these techniques can trace the memory patterns which are longer, concealed in the pre-earthquake time sequence. To study the fluctuations in earthquake related geoelectrical signals, the MFDFA algorithm have been applied by Telesca *et.al*[33]. The geophysical phenomenon is very complex and the earthquake-related geoelectrical variability is concealed by it and is conducted by completely unknown physical laws. The authors have shown that by means of Multifractal parameters, maximum asymmetry, width and range, the Multifractal analysis has led to a better understanding of the complexity. The Multifractility is mainly due to different long range correlations for small and large fluctuations. This was reported after considering worldwide data set of 91 Rn anomalies and randomly shuffling the surrogate series data. The multifractal singularity spectrum and the spectral width generated from therein helped in identifying the complexity values associated with each signal. Temporal correlations and Multifractal properties of long river discharge records were investigated around the globe from 41 hydrological stations by Bunde *et.al*[34]. It was obtained that all the 41 records of Multifractal spectra can be explained by a 'universal' function $\tau(q)$, obtained from a generalization of the fluctuation exponent H and the width $\Delta\alpha$ of the singularity spectrum respectively.

In many earlier works, the outcomes of inconsistency of soil radongot from Kolkata [22°32′N and 88°24′E] and Jalpaiguri (26°32′N, 88°46′E) were reported[35,36]. The previous study on Kolkata region provided interesting results on the use of Rn fluctuation as an indicator of pre-seismic event, in spite of Kolkata which is not being located in seismically active fault zone. For comparing to the results of Kolkata, a new project was started at Jalpaiguri, West Bengal, and it is located in a zone which is seismically active. It was seen that in the Jalpaiguri site, the average of the radon contamination was over the top, approximately near the factor of 40, thus more conclusively establishing the use of Rn gas anomaly as a precursor to earthquake, and its use as an earthquake surveillance monitor.

Here, the scrutiny of Rntime series data for the last 10 years viz. September 2005 to August 2014 have been studied in the perspective of chaos based methods in nonlinear scenario to obtain reliable and precise information. Very few works have been reported where study of radon concentration and local climatic parameters were made, Moreover, the methods used in these studies did not use nonlinear techniques essential for this kind of study. We analyze soil radon anomaly time series with MFDFA technique and also try to correlate the radon anomaly with that of temperature and relative humidity data using Multifractal cross correlation (MFDXA) technique.

Experimental Details: Rn monitoring is done here by using a track etch method of cellulose nitrate film with the help of CR-39plates which isa Solid State Nuclear Track Detector (SSNTD). The name of this allyl diglycol polycarbonate ($C_{12}H_{18}O_7$) has been abbreviated from 'Columbia Resin', registered type no. 39. The CR-39 plates having size 1cm by1 cm is slit and attached to the extremity of a cup having a tap and enclosed with acytomembrane which permits only Rn gas to

proceed. The dimensions of the cup are as follows: Height is taken as 4.7 cm, Diameter is taken as 6.3cm and 5.9 cm at the open end and at the closed end respectively. The cup containing the SSNTDs is placed in a metal container (with both ends open) kept 70 cm inside earth surface. A layer of silica gel around the cup absorbs the moisture on the surface. In an undisturbed ambiance, exposing of the CR-39 plates are done for 48 hours and the plates are subjected to chemical etching. Etching of the plates are done in 6N NaOH solution; the time needed is 6 hours and the temperature needed is 70°C. The alpha particle tracks in the plates are scanned by Carl Zeiss Jenaval microscope by using 10x objective in concurrence with 10x optic lens. The no. of tracks/cm^2 for Radon is calculated in this manner.

Methodology

The fractal techniques have been applied as per the methodology given in our book "Musicality of Human Brain through Fractal Analytics"[37].

Detrended Fluctuation Analysis (DFA): There are total five steps involves in the generalized multifractal DFA (MF-DFA) procedure. Among them the first three steps are homogeneous to the conventional DFA procedure. Let us assume[x_1, x_2,...,x_N]be a time series of length N and it is non-stationary.

Step 1: The first step involves changing the type of the as follows:

$$Y(i) = \sum (x_k - \bar{x}) \quad (1)$$

Where average value of the signal is represented by $\bar{x}$.

Step 2: The integration reduces the finite data and the measurement level noise present in the experimental records. The entire length of the signal consists of certain no. of samples has been bisected into Ns number of sections. Then for sample size s and total length N of the signal, the segments are

$$Ns = \text{int}\left(\frac{N}{s}\right) \quad (2)$$

Step 3: The function *F(s,v)* is of size *s* and for any sample it is the local RMS dissimilarity:

$$F^2(s,v) = \frac{1}{s}\sum_{i=1}^{s}\{Y[(v-1)s+i] - y_v(i)\}^2 \quad (3)$$

Step 4: The fluctuation function $F_q(s)$ having the q-th form is represented as follows:

$$F_q(s) = \left\{\frac{1}{Ns}\sum_{v=1}^{Ns}[F^2(s,v)]^{\frac{q}{2}}\right\}^{\left(\frac{1}{q}\right)} \quad (4)$$

where q is an index and except zero which can take all possible values. Because if q = 0 then the factor 1/q is infinite. This procedure can be repeated by varying the value of s.

Step 5: The scaling behavior of the fluctuation function is obtained by the relation

$$F_q(s) \sim s^{h(q)} \quad (5)$$

where h(q) is called the generalized Hurst exponent and can be expressed as the slope of a double logarithmic plot. The monofractal scaling exponent α is obtained for q=2. A time series which is monofractal in nature is specified by unique h(q) for all values of q. The autocorrelation properties of the signal are represented by parameter α which is also called as scaling exponent. By following the NBT algorithm, DFA technique was applied, which gives a perceptible measure of long range temporal correlation (LRTC) which exists in the time series[38].

Scaling exponents having value greater than 0.5 and less than 1 will be created by power-law behaviour when applied to any time series data having temporal correlation of long range order. In the time series the LRTC are more persistent i.e. decaying more slowly with time when the scaling exponent increases from 0.5 to 1. When the scaling exponent having a value greater than 1, power law behaviour is not revealed by the LRTC for a long time. Finally, when the scaling exponent = 1.5, this specifies Brownian noise andit is the integration of white noise. For all the Rn time series data, the DFA scaling exponent α values were figured out from eq. (5)

Figure-1: Experimental Setup.

Multifractal DFA (MFDFA): Most of the time series signals that we observe in daily life can hardly be characterized by using a single scaling exponent; hence the need arises to quantify them using multiple scaling exponents based on their scaling properties. The Multifractal Detrending algorithm (MFDFA) was detailed as an offshoot of DFA while catering different scaling ratios[39], for these more practical cases. The standard DFA procedure is reclaimed by putting q = 2 in **eqn. (5)**.Our keen interest isto observe how the fluctuation functions $F_q(s)$ which is q dependent, rely on the time scale s for different values of q. Hence, from step 2 to step 4must redo for several time scales s. It is clearly visible that $F_q(s)$ will increase as s increases. Again, on the Detrended Fluctuation Analysis having order m,F_q (s) is dependent of and for s ≥ m+ 2,$F_q(s)$ is explained only by construction. Again, with distinct values of q, the earlier step is repeated.

Step 5: The double logarithmic plot of $F_q(s)$ vs. s for each value of qanalyses the scaling pattern of fluctuation functions. Now, according to power-law,$F_q(s)$ rises for large values of s, if the series x_i is long-range power-law correlated.

$$F_q(s) \sim s^{h(q)} \tag{6}$$

The exponent h(q) depends on q generally. h(2) is identical with the Hurst exponent H for a stationary time series,. Thus the function h(q) is called as the generalized Hurst exponent.

The relation between the generalized Hurst exponent h(q) of MFDFA and the classical scaling exponent τ(q) is as follows:

$$\tau(q) = qh(q) - 1 \tag{7}$$

A monofractal series with long range correlation is specified by a single Hurst exponent H, while multifractal time series signal possess multiple Hurst exponents dependent on q.

The relation between singularity spectrum f(α) and h(q) is given as follows

$$\alpha = h(q) + qh'(q) \tag{8}$$

$$f(\alpha) = q[\alpha - h(q)] + 1 \tag{9}$$

Where α denotes the singularity power or Holder exponent and *f(α)* specifies the acreage corresponding to the subset sequence that is specified by α. The span of the multifractal spectrum manifests the extent of scaling exponents. Quantitatively the spectra can be categorized by using least square method suitable to a quadratic function[40]in the neighbourhood of extreme α_0 ,

$$f(\alpha) = P(\alpha - \alpha_0)^2 + Q(\alpha - \alpha_0) + R$$

Where R is an add-on constant, $R = f(\alpha_0) = 1$ and $Q = 0$ for a magnificently consistent spectrum which measures the asymmetry value for the spectrum. The spectral width can be calculated by hypothesizing the appropriate quadratic curve to zero.

Multifractal spectral span W is explained as follows,

$$W = \alpha_1 - \alpha_2$$

With $f(\alpha_1) = f(\alpha_2) = 0$

The span of the parabola has given by the measurement of the entanglement of the signal. As W increases, the multifractality of the time series rises. For a monofractal time series, as h(q) does not depend on q, the width has a value equal to zero. The origin of multifractality has been verified by the arbitrary shambling of the Rn time series data. Random shuffling of the raw data destroys all the correlations present in the signal which are of long range order by giving a completely uncorrelated signal in return. Thus a non-fractal scaling will be displayed by the shuffled data when subjected to multifractal analysis technique.

For the10 points of *q* which were in between −5 to +5, variation function *Fq*(*s*) was acquired which is of *q*th order. For demolishing all the correlations present in the data which are of long range order, the values of time series have been randomly shuffled and the remaining part is the totally uncorrelated sequence. For the scales varying from 16 to 1024,in the plot for theRn time series, the regression double logarithmic scenario of ln (*Fq*(*s*)) vs. ln(*s*) averaging for divergentmerits of q [from q= -3 to q= + 3] has been representedwhich is given in Figure-2(a-b). The value of *h*(*q*)achieves from the slope of the best suitable line obtained from the double logarithmic scenario of ln(*Fq*(*s*)) vs. ln(*s*). From Figure-2(b), it can be seen that with the changes in q, the time series has independents hambled values and thus having a definite slope[h(q)=H]for monofractal time series, which is the nothing but the Hurst exponent.

Figure-3(a) shows the dissimilarities of *h* (*q*) with *q* for Rn time-series for representative purpose. It is evident that the h (q) decreases with the increase of q, giving a proof of multifractal scaling in the Rn time series data. While for all values of q, the shuffled series shows a single value of h(q), while with q, the original Rn time series has varying values of h(q). As said earlier, from the span of the multifractal spectrum [f(α) vs α],the evaluation of the amount of multifractality present in the time series of various climatic parameters quantitatively is obtained. The original span of the signal is bigger than the shuffled span always and that can be seen from Figure-3(b). The shuffled series will show a peak nearby of 0.5at α_0, in the plot of f(α) vs. α, if monofractal nature exists in the shuffled data.

The detrended cross-correlation analysis (DCCA) investigates the long-term cross-correlations between two non-stationary time series[41-44]. The multifractal features of two cross-correlated signals can be revealed by the Multifractal Detrended Cross-Correlation Analysis (MF-DXA)[45-48].

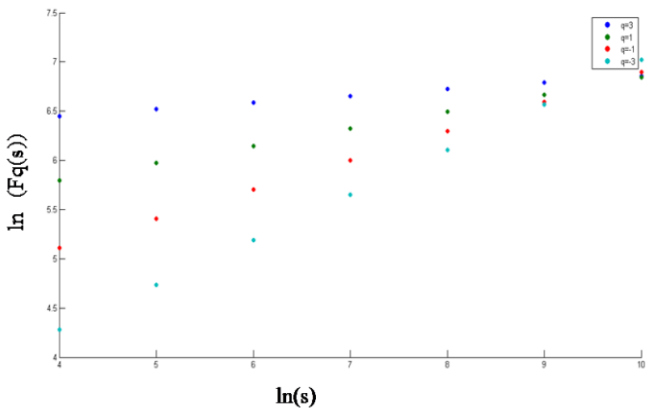

Figure-2(a): double logarithmic plot of Fq(s) vs. sfor Rn time series.

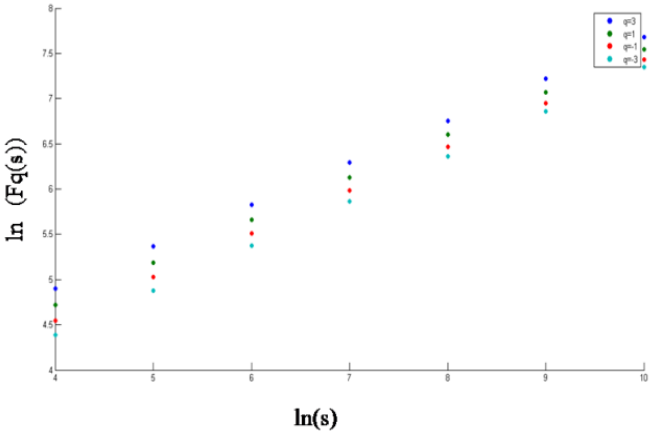

Figure-2(b): double logarithmic plot of Fq(s) vs. s for the shuffled data

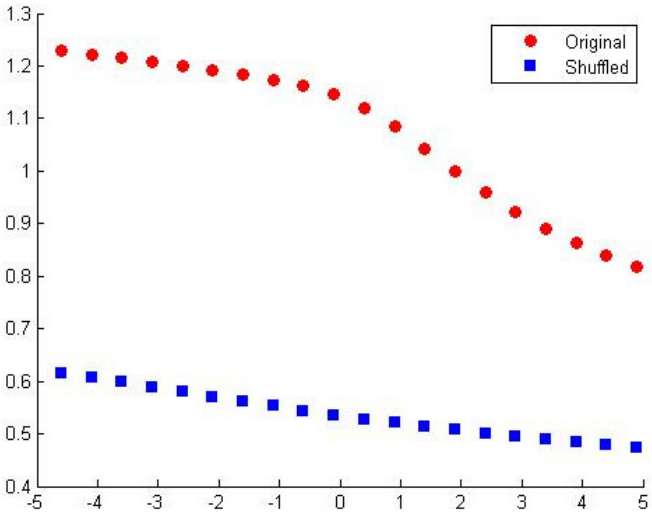

Figure-3(a): The dissimilarity ofh(q) the Hurst exponent with the scaling parameter q and.

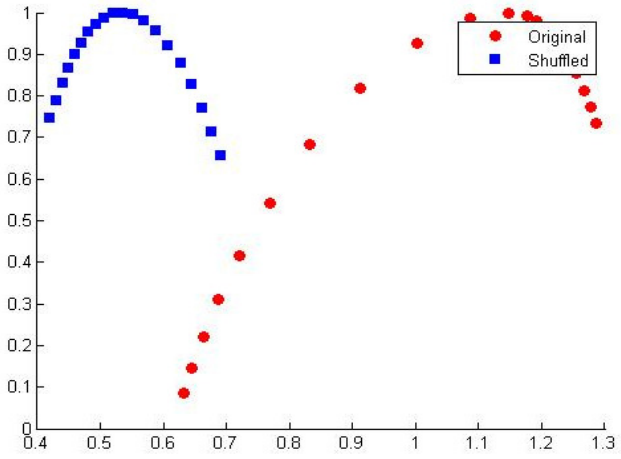

Figure-3(b): f (α) Vs α curve for indigenous and shambled Rn time sequence.

Multifractal Detrended Cross-Correlation Analysis (MFDXA): MFDXA method is a branch of the generalized MFDFA method[26]. Two data series x(i) and y(i) are represented here as

$X(i) \equiv [\sum_{k=1}^{i} x(k) - x_{avg}]$ for i = 1 . . . N (10)

$Y(i) \equiv [\sum_{k=1}^{i} x(k) - x_{avg}]$ for i = 1 . . . N

The following algorithm is similar to MFDFA method, just that we have to take $2N_s$ bins here. After averaging over 2Ns bins,we have got the qth order covariance Fq(s).

$$F_q(s) = \{1/2N_s \sum_{v=1}^{2Ns} [F(s,v)]^{q/2}\}^{1/q} \quad (11)$$

Fq(s) increases as s increases, power law behaviour will represent by the function Fq(s) in the form

$F_q(s) \sim s^{\lambda(q)}$.

By taking λ(q) as the slope, ln F_q will rests on ln s linearly if such scaling exists. The degree of cross-correlation in between the two time series is denoted by the scaling exponent λ(q). λ(q) rests on q in general. As F_q blows up at q = 0,it is not possible to get the value of λ(0) directly. A logarithmic averaging procedure is applied to get Fq instead of the normal averaging procedure

$$F_0(s) = \{1/4N_s \sum_{v=1}^{2Ns} [F(s,v)]\} \sim s^{\lambda(0)}. \quad (12)$$

The method reduces to standard DCCA for q = 2. Ifλ(q) the scaling exponentdoes not depend on q, then between the two time series, there exists the monofractal cross-correlations. On the contrary, if the scaling exponent λ(q) depends on q, the multifractal cross-correlations exists between two time series. Among the two time series x(i) and y(i), the degree of cross-correlation is denoted by the scaling exponent λ(q).

The auto-correlation function is as follows:

$C(\tau) = \langle [x(i+\tau) - \langle x \rangle][x(i) - \langle x \rangle] \rangle \sim \tau^{-\gamma}$. (13)

The cross-correlation function is as follows:

$$C_x(\tau) = \langle [x(i+\tau) - \langle x \rangle][y(i) - \langle y \rangle] \rangle \sim \tau^{-\gamma_x} \quad (14)$$

Where γ and γ_x respectively denotes auto-correlation and cross-correlation exponents. Due to the superimposing of uneven and drifts on the composed data, usually straight calculation of these exponents are not proposed; rather the Detrended Fluctuation Analysis method is the authentic method to compute auto-correlation exponent, namely $\gamma = 2 - 2h$ $(q = 2)$[49]. The relation between cross-correlation exponent, γ_x and scaling exponent $\lambda(q)$ is as follows: $\gamma_x = 2 - 2\lambda(q = 2)$[50]. γ_x= 1for non-correlated data while γ_x= -1 for a strongly correlated data. Thus, the data is more correlated as lower as the value of γ and γ_x.

With q, for the two particular samples Rn concentration and temperature, Figure-4 describes the dissimilarity of cross correlation scaling exponent λ (q). The two samples separately obtained from MFDFA technique, the dissimilarity between h (q) and q have been represented in the same stature for comparison. The figure clearly represents that the cross-correlated signal also shows multifractal behavior just like the individual signals.

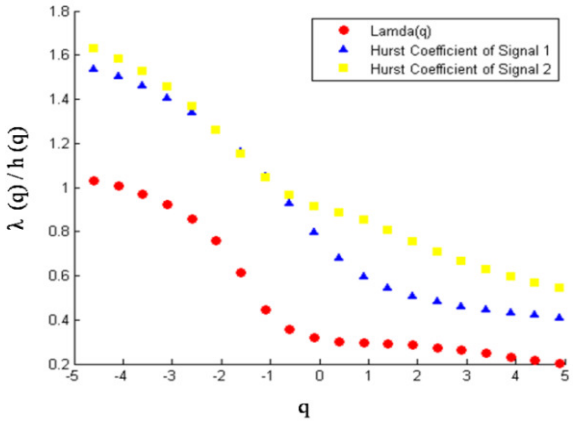

Figure-4: The dissimilarity of λ (q) and h (q) for two time series Rn concentration and temperature.

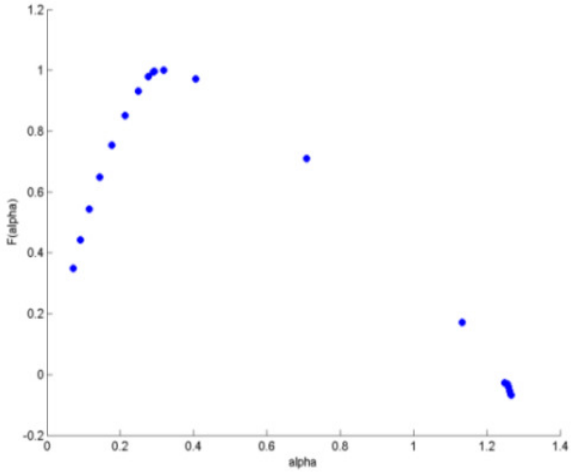

Figure-5: Sample Rn and temperature's Multifractal cross-correlated Spectrum.

The multifractal spectrum of the cross correlated sample of Rn and temperature time series have been plotted in Figure-5. This particular figure represents the amount of multifractality present in the cross-correlated sample even. In this paper, though we are primarily concerned with how the values of γ_x change for different local climatic parameter and soil radon fluctuation, the amount of multifractality present in these cross-correlated signals will be dealt with in a forthcoming study. In the Results and Discussion section, we will elaborate on how the degree of cross-correlation, γ_x varies for different time series combinations and what impact it has on the climatic outcomes that we see in the Universe.

Results and discussion

The following figures show the time series of Rn concentration, temperature, humidity and rainfall for the last 10 years.

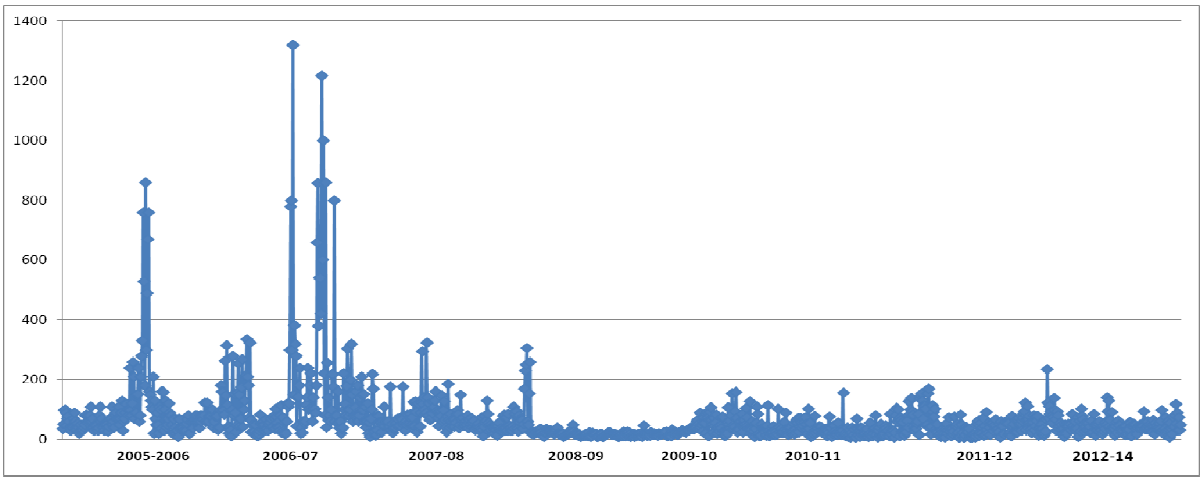

Figure-6: Rn concentration time series for the last ten years.

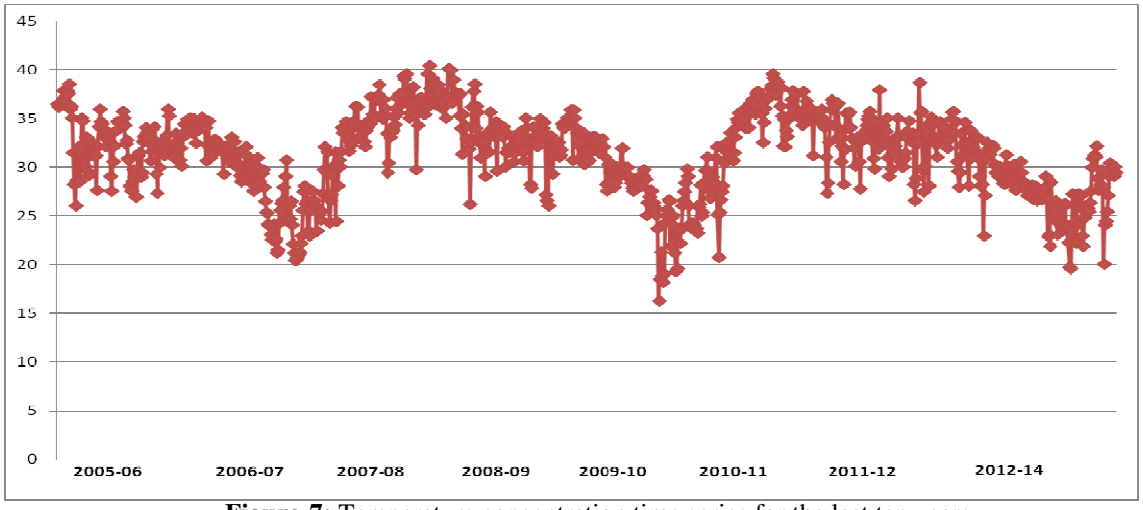

Figure-7: Temperature concentration time series for the last ten years.

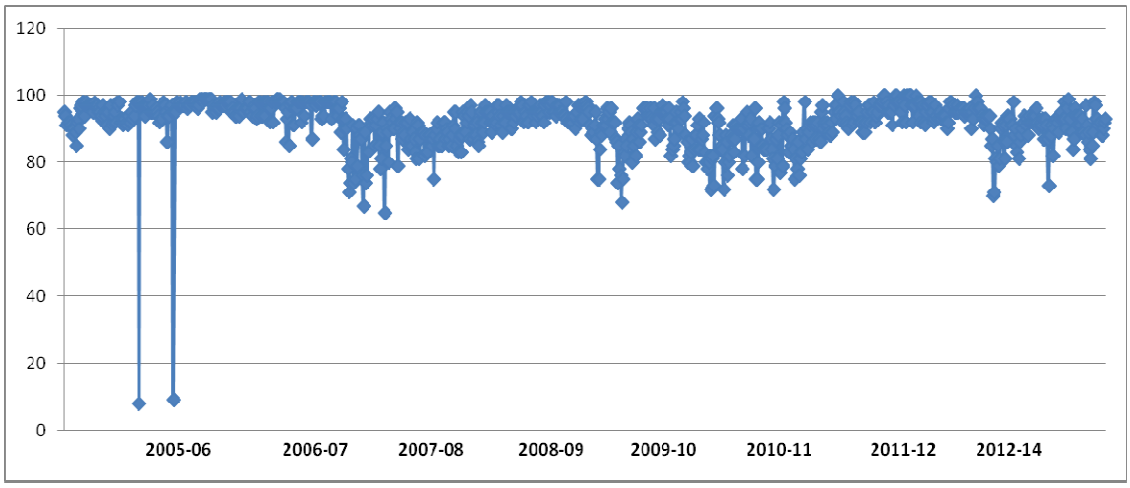

Figure-8: Humidity concentration time series for the last ten years.

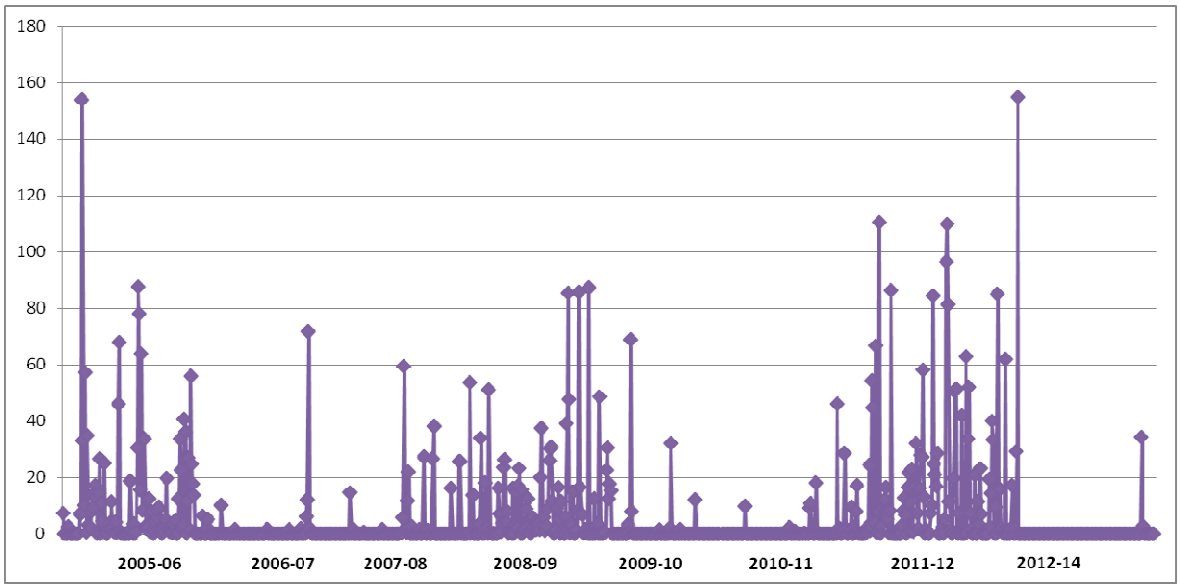

Figure 9: Rainfall concentration time series for the last ten years.

From the time series analysis of Rn count, temperature variation, humidity and rainfall concentration, we have evaluated the Hurst exponent, multifractal width and autocorrelation exponent corresponding to each of the time series. The long range temporal correlations present in the time series has been reflected by the Hurst exponent, while the complicated values related to the time series are given by the multifractal spectral width. A measure of the self-correlation in the time series is nothing but the autocorrelation exponent. Table-1 gives the measures of Hurst Exponent, autocorrelation and multifractal width of the different time series.

Table-1: The variation of auto-correlation, DFA exponent and Multifractal spectral width within 2005-2014.

	Rn Count	Temperature	Humidity	Rainfall
Hurst Exponent	1.095	1.266	0.917	0.996
Auto correlation	0.668	0.545	0.463	0.386
Multifracta l Width	0.715	0.913	0.589	0.653

From Table-1, we have plotted the corresponding bar graphs which depict the variation of different measurement parameters. The SD values have been shown in the form of error bars corresponding to each of the parameter which essentially denotes the computational error corresponding to each of the measurements. Figure-10 represents the variation of specific parameters.

This investigation of Rn time series function for 10 years and local climate parameters with nonlinear rigorous approach reveals: i. All the time series used herein, i.e. Rn, temperature, humidity, rainfall are multifractal in nature with different multifractal widths i.e. of varying complexity, ii. Also, all the time series are auto-correlated with different values, iii. Both the Hurst Exponent and multifractal spectral width show values on the higher side for temperature variation and rainfall.

Next, by using the MFDXA technique, the cross-correlation coefficient has been assessed, corresponding to each pair of local climatic parameters. The degree of correlation subsists between the two climatic parameters has been measured by the cross-correlation coefficient γ_x and may thus be considered as a very important measure of how the change in one parameter affects the other. This may be considered very crucial while developing an automated earthquake surveillance system. The MFDXA technique goes into such depths of the complex geo-physical time series, just like a mathematical microscope which is not possible by any other methods. Table-2 represents the cross-correlation coefficients corresponding to different pairs of climatic parameters as measured in our experiment.

Table-2: Multifractal Detrended Cross Correlation of Radon concentration with Temperature, Humidity, Rain fall within 2005-2014.

	Cross-correlation Coefficient (γ_x)
Rn Count vs Temperature	-0.692
Temperature vs Humidity	0.163
Rn Count vs Humidity	-0.327
Rn Count vs Rainfall	-0.018
Temperature vs Rainfall	0.278
Humidity vs Rainfall	0.115

Figure-11 illustrates the findings of Table-2, where the error bars correspond to standard computational errors in each of the measurement.

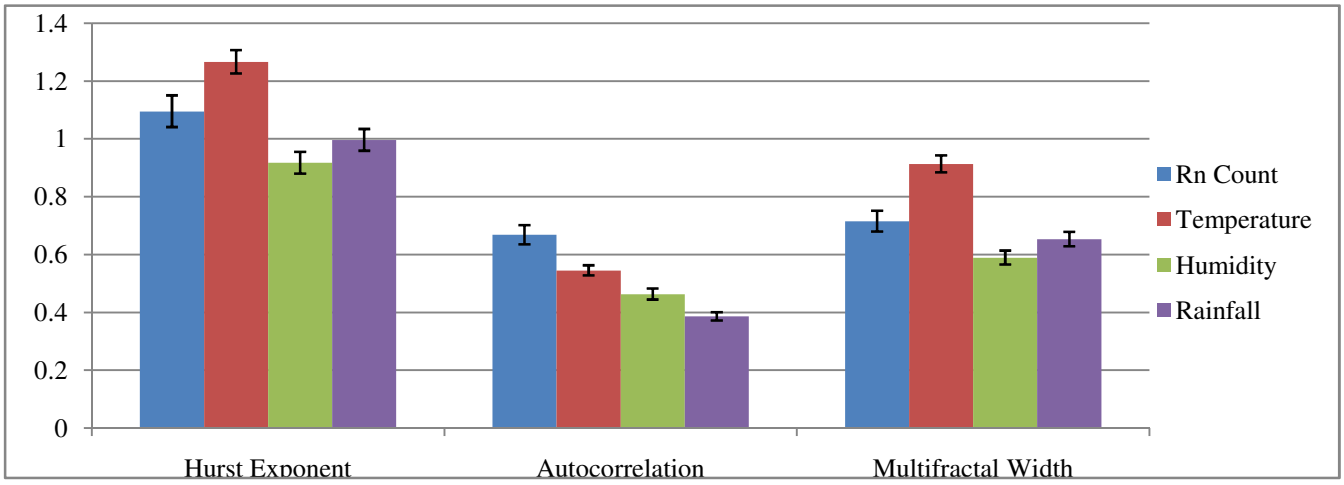

Figure-10: Graph showing the scaling parameters for Rn, temperature, rainfall and humidity.

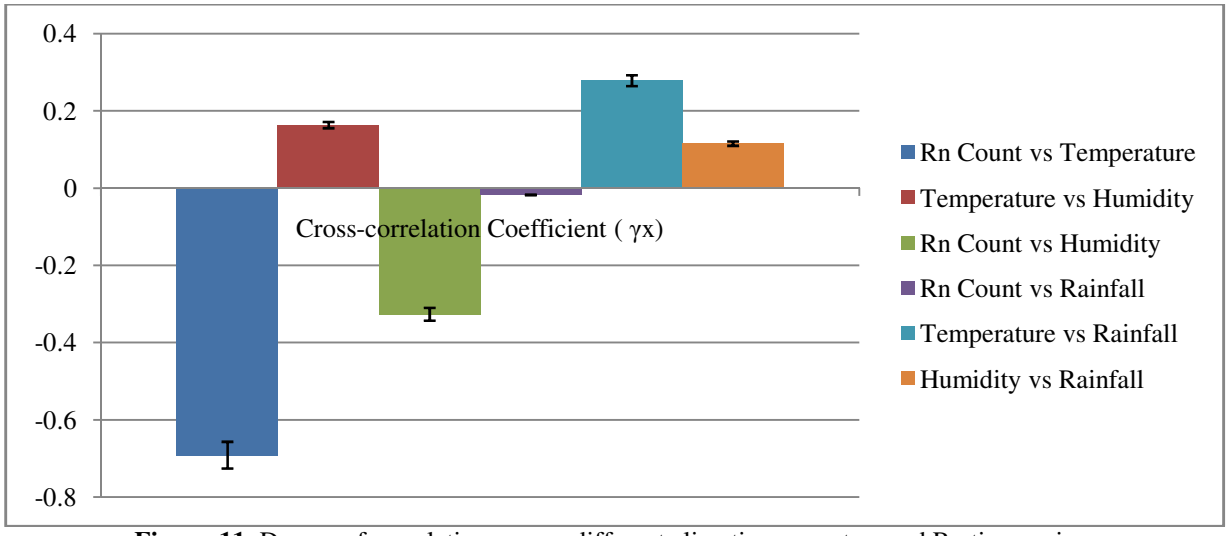

Figure-11: Degree of correlation among different climatic parameters and Rn time series.

As pointed out earlier, as the value of cross-correlation coefficient decreases, the degree of correlation between the two time series signals increases. It can be seen from Figure-11 that soil Rn emission is strongly correlated with local climate parameters including temperature, rainfall and humidity. Maximum cross-correlation occurs between Rn emission and temperature as values of cross-correlation coefficient is minimum in this case.

Conclusion

Since local climate parameters play a significant role in emission of soil radon, before use of this time series for earthquake surveillance, this observation should be taken care of judicially. As discussed earlier, Radon fluctuation happens to be most sensitive and useful parameter for seismic surveillance. Many time series of Rn has been used for identifying earthquakes. This study with rigorous methods should be taken care of as a caution before confident identification of occurrence of earthquakes.

Acknowledgement

Shankha Sanyal is grateful to Council of Scientific and Industrial Research (CSIR), Govt. of India for providing the CSIR-Senior Research Fellowship (SRF) for continuing his research work (09/096(0876)/2017-EMR-I).

References

1. Nazaroff W. and Nero A. (1988) Radon and its decay products in indoor air. Wiley, New York.

2. Vogiannis E. and Nikolopoulos D. (2015). Radon sources and associated risk in terms of exposure and dose. *Front Pub Heal Env Heal*, 2, 1-10.

3. Nikolopoulos D. and Louizi A. (2008). Study of indoor radon and radon in drinking water in Greece and Cyprus: implications to exposure and dose. *Rad Meas*, 43(7), 1305-1314.

4. Planinic J., Radolic V. and Culo D. (2000). Searching for an earthquake precursor: Temporal variations of radon in soil and water. *Fizika B*, 75-82.

5. Garavaglia M., Braitenberg C. and Zadro M. (1998). Radon monitoring in a cave of North-Eastern Italy. *Physics and Chemistry of the Earth*, 23(9-10), 949-952.

6. Talwani P. (1979). An empirical earthquake prediction model. *Phys Earth Planet Inter*, 18(4), 288-302.

7. Ramola R.C., Singh S. and Virk H.S. (1988). A model for the correlation between radon anomalies and magnitude of earthquakes. *International Journal of Radiation Applications and Instrumentation*. Part D. Nuclear Tracks and Radiation Measurements, 15(1-4), 689-692. DOI: 10.1016/1359-0189(88)90229-4.

8. Swakoń J., Kozak K., Paszkowski M., Gradziński R., Łoskiewicz J., Mazur J. and Olko P. (2005). Radon concentration in soil gas around local disjunctive tectonic zones in the Krakow area. *Journal of Environmental Radioactivity*, 78(2), 137-149.

9. Singh M., Kumar M., Jain R.K. and Chatrath R.P. (1999). Radon in ground water related to seismic events. *Radiation Measurements*, 30(4), 465-469.

10. Amrani D., Cherouati D.E. and Cherchali M.E.H. (2000). Groundwater radon measurements in Algeria. *Journal of Environmental Radioactivity*, 51(2), 173-180.

11. Alekseev V.A., Alekseeva N.G. and Jchankuliev J. (1995). On relation between fluxes of metals in waters and radon in Turkmenistan region of seismic activity. *Radiation Measurements*, 25(1-4), 637-639.

12. İnceöz M., Baykara O., Aksoy E. and Doğru M. (2006). Measurements of soil gas radon in active fault systems: a

case study along the North and East Anatolian fault systems in Turkey. *Radiation Measurements*, 41(3), 349-353.

13. Segovia N., Tamez E., Peña P., Carrillo J., Acosta E., Armienta M.A. and Iturbe J.L. (1999). Groundwater flow system in the valley of Toluca, Mexico: an assay of natural radionuclide specific activities. *Applied radiation and isotopes*, 50(3), 589-598.

14. Ilić R., Rusov V.D., Pavlovych V.N., Vaschenko V.M., Hanžič L. and Bondarchuk Y.A. (2005). Radon in Antarctica. *Radiation measurements*, 40(2-6), 415-422.

15. Segovia N., Mena M., Seidel J.L., Monnin M., Tamez E. and Pena P. (1995). Short and long term radon in soil monitoring for geophysical purposes. *Radiat. Meas.*, 25(1-4), 547-552.

16. Tsvetkova T., Przylibski Tadeusz, Nevinsky I. and Nevinsky V. (2005). Measurement of radon in the East Europe under the ground. *Radiation Measurements*, 40(1), 98-105.

17. King C.Y. (1978). Radon emanation on San Andreas fault. *Nature*, 271, 516-519.

18. Hauksson E. (1981). Radon content of groundwater as an earthquake precursor: Evaluation of worldwide data and physical basis. *J. Geophys. Res*., 86(B10), 9397-9410.

19. Walia V., Bajwa B.S., Virk H.S. and Sharma N. (2003). Relationships between seismic parameters and amplitudes of radon anomalies in N–W Himalaya, India. *Radiat. Meas*., 36, 393-396.

20. Walia V., Virk H.S., Yang T.F., Mahajan S., Walia M. and Bajwa B.S. (2005). Earthquake prediction studies using radon as a precursor in N-W Himalayas, India: a case study. *Terr. Atmos. Ocean. Sci.*, 16, 775-804.

21. Das N.K., Chaudhuri H., Bhandari R.K., Ghose D., Sen P. and Sinha B. (2006). Continuous monitoring of Rn222 and its progeny at a remote station for seismic hazard surveillance. *Radiat. Meas*, 41, 634-637.

22. Ramola R.C., Prasad Y., Prasad G., Kumar S. and Choubey V.M. (2008). Soil-gas radon as seismotectonic indicator in Garhwal Himalaya. *Applied Radiation and Isotopes*, 66(10), 1523-1530.

23. Barman C., Chaudhuri H., Deb A., Ghose D. and Sinha B. (2015). The essence of multifractal detrended fluctuation technique to explore the dynamics of soil radon precursor for earthquakes. *Natural hazards*, 78(2), 855-877.

24. Reddy D.V., Nagabhushanam P., Sukhija B.S. and Reddy G.R. (2010). Continuous radon monitoring in soil gas towards earthquake precursory studies in basaltic region. *Radiat. Meas*., 45(8), 935-942.

25. Deb A., Gazi M. and Barman C. (2016). Anomalous soil radon fluctuations–signal of earthquakes in Nepal and eastern India regions. *Journal of Earth System Science*, 125(8), 1657-1665.

26. Zhou W.X. (2008). Multifractal detrended cross-correlation analysis for two nonstationary signals. *Physical Review E*, 77(6), 066211.

27. Mandelbrot B.B. (1982). The fractal geometry of nature. New York: WH freeman, 1.

28. Petraki E., Nikolopoulos D., Fotopoulos A., Panagiotaras D. and Koulouras G. (2013). Self-organised critical features in soil radon and MHz electromagnetic disturbances: Results from environmental monitoring in Greece. *App Rad Isot*, 72, 39-53.

29. Nikolopoulos D., Petraki E., Vogiannis E., Chaldeos Y., Yannakopoulos P., Kottou S. and Stonham J. (2014). Traces of self-organisation and long-range memory in variations of environmental radon in soil: Comparative results from monitoring in Lesvos Island and Ileia (Greece). *Journal of Radioanalytical and Nuclear Chemistry,* 299(1), 203-219.

30. Eftaxias K., Balasis G., Contoyiannis Y., Papadimitriou C., Kalimeri M., Athanasopoulou L., Nikolopoulos S., Kopanas J., Antonopoulos G. and Nomicos C. (2010). Unfolding the procedure of characterizing recorded ultra low frequency, kHZ and MHz electromagnetic anomalies prior to the L'Aquila earthquake as pre-seismic ones-Part 2. *Natural Hazards and Earth System Sciences*, 10(2), 275-294.

31. Eftaxias K. (2010). Footprints of nonextensive Tsallis statistics, selfaffinity and universality in the preparation of the L'Aquila earthquake hidden in a pre-seismic EM emission. *Physica A: Statistical Mechanics and its Applications*, 389(1), 133-140.

32. Nikolopoulos D., Petraki E., Nomicos C., Koulouras G., Kottou S. and Yannakopoulos P.H. (2015). Long-memory trends in disturbances of radon in soil prior to the twin ML= 5.1 earthquakes of 17 November 2014 Greece. *J. Earth Sci. Climatic Change*, 6(1), 1-10.

33. Telesca L., Lovallo M., Lapenna V. and Macchiato M. (2007). Long-range correlations in two-dimensional spatio-temporal seismic fluctuations. *Physica A: Statistical Mechanics and its Applications*, 377(1), 279-284.

34. Koscielny-Bunde E., Kantelhardt J.W., Braun P., Bunde A. and Havlin S. (2006). Long-term persistence and multifractality of river runoff records: Detrended fluctuation studies. *Journal of Hydrology*, 322(1-4), 120-137.

35. Ghosh D., Deb A., Sengupta R., Patra KK. and Bera S. (2007). Pronounced soil-radon anomaly—Precursor of recent earthquakes in India. *Radiation Measurements*, 42 (3), 466-471.

36. Ghosh D., Deb A., Sengupta R., Bera S., Sahoo S.R., Haldar S. and Patra K.K. (2011). Comparative study of seismic surveillance on radon in active and non-active tectonic zone of West Bengal, India. *Radiation Measurements*, 46(3), 365-370.

37. Ghosh D., Sengupta R., Sanyal S. and Banerjee A. (2018). Musicality of Human Brain Through Fractal Analytics. Springer Singapore.

38. Hardstone R., Poil S.S., Schiavone G., Jansen R., Nikulin V.V., Mansvelder H.D. and Linkenkaer-Hansen K. (2012). Detrended fluctuation analysis: a scale-free view on neuronal oscillations. *Frontiers in physiology*, 3, 450.

39. Kantelhardt J.W., Zschiegner S.A., Koscielny-Bunde E., Havlin S., Bunde A. and Stanley H.E. (2002). Multifractal detrended fluctuation analysis of nonstationary time series. *Physica A: Statistical Mechanics and its Applications*, 316(1), 87-114.

40. Figliola A., Serrano E., Rostas J.A.P., Hunter M. and Rosso O.A. (2007). Study of EEG brain maturation signals with multifractal detrended fluctuation analysis. AIP Conference Proceedings, AIP, 913(1), 190-195.

41. Podobnik B. and Stanley H.E. (2008). Detrended cross-correlation analysis: A new method for analyzing two nonstationary time series. *Physical Review Letters*, 100(8), 084102.

42. Podobnik B., Horvatic D., Ng A.L., Stanley H.E. and Ivanov P.C. (2008). Modeling long-range cross-correlations in two-component ARFIMA and FIARCH processes. *Physica A: Statistical Mechanics and its Applications*, 387(15), 3954-3959.

43. Podobnik B., Grosse I., Horvatić D., Ilic S., Ivanov P.C., and Stanley H.E. (2009). Quantifying cross-correlations using local and global detrending approaches. *The European Physical Journal B*, 71(2), 243-250.

44. Xu N., Shang P. and Kamae S. (2010). Modeling traffic flow correlation using DFA and DCCA. *Nonlinear Dynamics*, 61(1-2), 207-216.

45. He L.Y. and Chen S.P. (2011). Multifractal detrended cross-correlation analysis of agricultural futures markets. *Chaos, Solitons and Fractals*, 44(6), 355-361.

46. Jiang Z.Q. and Zhou W.X. (2011). Multifractal detrending moving-average cross-correlation analysis. *Physical Review E*, 84(1), 016106.

47. Wang F., Liao G.P., Zhou X.Y. and Shi W. (2013). Multifractal detrended cross-correlation analysis for power markets. *Nonlinear Dynamics*, 72(1-2), 353-363.

48. Ghosh D., Dutta S. and Chakraborty S. (2014). Multifractal detrended cross-correlation analysis for epileptic patient in seizure and seizure free status. *Chaos, Solitons and Fractals*, 67, 1-10.

49. Movahed M.S. and Hermanis E. (2008). Fractal analysis of river flow fluctuations. *Physica A: Statistical Mechanics and its Applications*, 387(4), 915-932.

50. Podobnik B., Jiang Z.Q., Zhou W.X. and Stanley H.E. (2011). Statistical tests for power-law cross-correlated processes. *Physical Review E*, 84(6), 066118.

51. Feder J. (2013). Fractals. Springer Science and Business Media.